26

Machining with Flexible Manipulators: Critical Issues and Solutions

Jianjun Wang, Hui Zhang, Zengxi Pan
ABB Corporate Research Center
2000 Day Hill Road, Windsor, CT, USA 06095

1. Introduction

The automotive industry represents the fastest-growing market segment of the aluminium industry, due to the increasing usage of aluminium in cars. The drive behind this is not only to reduce the vehicle weight in order to achieve lower fuel consumption and improved vehicle performance, but also the desire for more sustainable transport and the support from new legislation. Cars produced in 1998, for example, contained on average about 85 Kg of aluminium. By 2005, the automotive industry will be using more than 125 Kg of aluminium per vehicle. It is estimated that aluminium for automotive industry alone will be a 50B$/year market.

Most of the automotive aluminium parts start from a casting in a foundry plant. The downstream processes usually include cleaning and pre-machining of the gating system and riser, etc., machining for high tolerance surfaces, painting and assembly. Today, most of the cleaning operations are done manually in an extremely noisy, dusty and unhealthy environment. Therefore, automation for these operations is highly desirable. However, due to the variations and highly irregular shape of the automotive casting parts, solutions based on CNC machining center usually presented a high cost, difficult-to-change capital investment.

To this end, robotics based flexible automation is considered as an ideal solution for its programmability, adaptivity, flexibility and relatively low cost, especially for the fact that industrial robot is already applied to tend foundry machines and transport parts in the process. Nevertheless, the foundry industry has not seen many success stories for such applications and installations. Currently, more than 80% of the application of industrial robots is still limited to the fields of material handling and welding. (Figure 1)

The major hurdle preventing the adoption of robots for material removal processes is the fact that the stiffness of today's industrial robot is much lower than that of a standard CNC machine. The stiffness for a typical articulated robot is usually less than 1 N/μm, while a standard CNC machine center very often has stiffness greater than 50 N/μm.

Most of the existing literature on machining process, such as process force modelling (Kim et al., 2003; Stein & Huh, 2002], accuracy improvement (Yang 1996) and vibration suppression (Budak & Altintas, 1998) are based on the CNC machine. Research in the field of robotic machining is still focused on accurate off-line programming and calibration (Chen & Hu, 1999; Sallinen & Heikkila, 2000; Wang et al., 2003a, 2003b). Akbari et al. (Akbari & Higuchhi, 2000) describe a tool angle adjustment method in a grinding application with a

Source: Industrial Robotics: Programming, Simulation and Applicationl, ISBN 3-86611-286-6, pp. 702, ARS/plV, Germany, December 2006, Edited by: Low Kin Huat

small robot. In that case the process force is very small. Matsuoka etc al (Matsuoka et al., 1999) study the characters of an articulated robot in a milling process avoiding large process force by using an end mill with small diameter and high spindle speed. Without the capability of real-time force control, the method to eliminate the force effect on the robotic machining process has not been fully addressed in the research community or in industry.

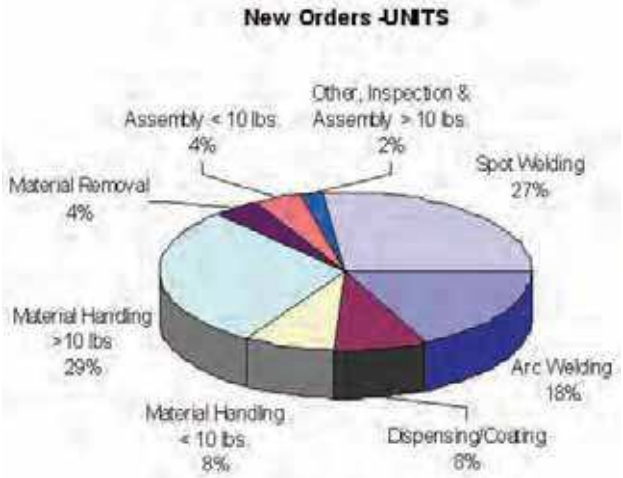

Fig. 1. 2003 Robot Applications in North America . A total of 12,367 robots valued at $876.5 million were ordered. When sales to companies outside North America are added in, the total for North American robotics suppliers is 12,881 robots valued at $913 million. NOTE: These numbers include results from North America and Outside North America. Source: Robotic Industries Association.

Machining processes, such as grinding, deburring, polishing, and milling are essential force tasks whose nature requires the robot end effector to establish physical contact with the environment and exert a process-specific force. The inherent lower stiffness of the robot has presented many challenges to execute material removal applications successfully. First and foremost, the lower stiffness makes chatter much easier to occur in robot than in CNC machine. Severe low frequency chatter has been observed in milling and deburring processes. Although extensive research on chatter has been conducted, none of the existing research has focused on chatter mechanism in robotic machining process. The result is that without a good understanding or even a rule of thumb guideline, robotic engineers and technicians have to spend tremendous time on trial and error for the sheer luck of stumbling a golden setup or has to sacrifice the productivity by settling on very conservative cutting parameters.

The second challenge is the structure deformation and loss of accuracy due to the required machining force. The predominant cutting action in machining involves shear deformation of the work material to form a chip. The contact between the cutting tool and the workpiece generates significant forces. As a result, a perfect robot program without considering contact and deformation will immediately become flawed as the robot starts to execute the machining task. Unlike multi-axis CNC machine centers, such deformation is coupled and varies even subjected to the same force in different workspace locations. Such coupling

results in deformation not only in the direction of reaction force and can generate some counter-intuitive results.
Lastly, the machining of casting parts presents a unique challenge with non-uniform cutting depth and width. In conventional robot programming and process planning practice, the cutting feed rate is constant even with significant variation of cutting force from part to part, which dictates a conservative cutting feed rate without violating the operational limits. Therefore, it is desirable to maximize the material removal rate (MRR) and minimize cycle time by optimizing the cutting feed rate based on a programmed spindle load. By optimizing the feed rate in real time, one could compensate for conservative assumptions and process variations to help reduce cycle time. Every part, including the first one, is optimized automatically, eliminating the need for manual part program optimization.
This chapter will address the above critical challenges with detailed experimental observation, in-depth analysis of underlying root causes, and practical solutions to improve stability, accuracy and efficiency (Pan et al., 2006; Zhang et al., 2005). If industrial robots could be made to provide the same performance under contact situations as that they already have, then robotic machining would result in significant cost savings for a lot of potential applications. Moreover, if such applications can be proven to be economically viable and practically reliable, one would expect to witness many success stories in the years to come. This chapter is organized in six sections including the introduction. Section II is devoted to the modelling of robotic machining process and serves as the basis for the following 3 sections, where chatter analysis, deformation compensation and MRR control are presented respectively. The whole chapter is then concluded in Section VI.

2. Modelling of Robotic Machining Process

Machining processes are essential force tasks which require the end effector of the robot to establish physical contact with the environment and exert a process-specific force. Characterization of the interaction bewteen the tool and the workpiece is essential for analyzing and solving the outstanding problems in robotic machining. For this purpose, a simplified interaction model is introduced here as the basis for the following sections.
As shown in figure 2, the dynamic interfaction in the machining processes is modelled as a closed loop connection between a force model of the machining process and a dynamic model of the machine tool-workpiece structure.

2.1 Robot-tool structure model

For a typical robotic machining workcell setup where the robot holds the spindle and the workpiece is mounted on a strong stationary foundation such as a steel table, the model of the machine tool-workpiece structure can be simplied as that of robot-tool structure due to the much larger stiffness of the workpiece-table strucutre. For an articulated 6-axis serial robot, the robot-tool structure is modeled by the transfer function in s domain and differential equation in time domain as:

$$\{\Delta\} = [G(s)]\{F\} \tag{1}$$

$$[M]\{\ddot{\Delta}\} + [C]\{\dot{\Delta}\} + [K]\{\Delta\} = \{F\} \tag{2}$$

where $[G(s)]$ is matrix of system transfer functions, $[M]$, $[C]$ and $[K]$ are 6×6 system mass, damping and stiffness matrix respectively. These matrixes are generally configuration dependent, but for the convenience of analysis, they can be treated as constant when robot only moves in a small range.

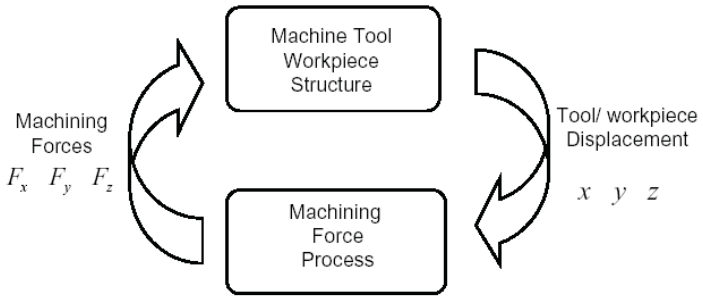

Fig. 2. Closed-loop model of dynamic interaction in the machining processes.

The mass matrix is related to robot rotational inertia in joint space as

$$M = J(Q)^{-T} I_q(Q) J(Q)^{-1} \tag{3}$$

Where Q is the joint angles, $J(Q)$ is the Jacobian matrix of the robot and $I_q(Q)$ is a 6×6 matrix representing the robot rotational inertia in joint space. $I_q(Q)$ is a function of joint angle and is not a diagonal matrix. It could be derived from robot kinematic model by Newton-Euler method or Lagrangian method, if the rigid body inertia parameters are available.

Similar to the mass matrix, stiffness matrix in Cartesian space K and joint space K_q are related by Jacobian matrix of robot as:

$$K = J(Q)^{-T} K_q J(Q)^{-1} \tag{4}$$

When the compliance of robot structure mostly comes from the deformation of gear box, the robot joint stiffness K_q can be modeled as a constant 6×6 diagonal matrix:

$$\tau = K_q \cdot \Delta Q \tag{5}$$

Where τ is the torque load on the six joints, ΔQ is the 6×1 deformation vector of all joints. This simplification is justifiable for industrial robots as they are designed to achieve high positioning accuracy and high strength. Elastic properties of the arms are insignificant. As result, the dominant contribution factor for a large deflection of the manipulator tip position is the joint compliance, e.g., due to gear transmission elasticity. Robot stiffness model could therefore be reduced to six rotational stiffness coefficients in the joint space. From the control point of view, this model is also easy to implement, since all industrial robot controllers are decoupled to SISO joint control at the servo level. Joint deformation could be directly compensated on the joint angle references passed to the servo controller.

Compared to CNC machines, articulated robots have totally different structural characteristics (table 1). First all, the serial structure of articulated robot has a much lower stiffness than that of a standard CNC machine. The stiffness for an articulated robot is usually less than 1 N/μm, while a standard CNC machine very often has stiffness greater than 50 N/μm. Secondly, with a large mass, the base natural frequency of robot structure is very low. Typical for a large robot, it is around 10Hz compared with several hundred Hz or

even more than one thousand Hz for the moving component of a CNC machine. Lastly, the stiffness matrix of the robot is configuration dependent and nondiagonal. This means that, first, the force and deformation in Cartesian space is coupled, the force applied in one direction will cause the deformation in all directions/orientations; second, at different locations, the Cartesian stiffness matrix will take different values. As it will be shown in the following sections, a lot of unique problems present in robotic machining have to do with the low and coupled stiffness matrix.

2.86E+02	-8.78E+02	8.12E+02	1.49E+06	3.01E+05	3.97E+05
-8.78E+02	2.39E+02	5.48E+03	-1.85E+05	-5.46E+05	-4.09E+05
8.12E+02	5.48E+03	4.91E+02	-4.56E+06	4.31E+05	8.62E+05
1.49E+06	-1.85E+05	-4.56E+06	7.53E+07	5.85E+08	-7.62E+08
3.01E+05	-5.46E+05	4.31E+05	5.85E+08	1.68E+08	3.20E+08
3.97E+05	-4.09E+05	8.62E+05	-7.62E+08	3.20E+08	1.30E+08

Table 1. One example of the Cartesian Stiffness Matrix (Units are N/mm, N/rad, N·mm/mm, and N·mm/rad respectively.)

2.2 Machining force model

Machining force results from the interaction between the tool and workpiece. It directly affects all facets of the machining operation. Accurate models are necessary to estimate force levels, spindle power requirements, etc. to aid the designer in planning the machining operation. A tremendous amount of effort has occurred in the area of cutting-force modeling over the past several decades. Models used for simulation purposes are often quite complex and incorporate effects such as tool and spindle run out, structural vibrations and their impact on the instantaneous feed, the effect of the cutting tool leaving the workpiece due to vibrations, intermittent cutting, tool geometry, etc. But for controller analysis and design, force model is typically very simple.

Throughout this chapter, the resultant machining force is represented as a static or a linear first-order model as:

$$F = K \cdot w \cdot d \cdot f \tag{6}$$

$$F = K \cdot w \cdot d \cdot f \frac{1}{\tau_m s + 1} \tag{7}$$

where w is width of cut, d is the depth of cut, f is the feed, K is machining coefficent dependent on workpiece material, tool shape, tool matrial and many other factors, τ_m is the machining process time constant. Since one spindle revolution is required to develop a full chip load, τ_m is 63% of the time required for a spindle revolution (Daneshmend & Pak, 1986). For industrial robot typical equipped with 10Hz bandwidth of servo loop, the force process gain may be seen as $\theta = K \cdot w \cdot d$, which is sensitive to the process inputs.

The force process in machining is actually a nonlinear system since the cutting parameters (feed, depth-of-cut, and width-of-cut) are related to machining force in a nonlinear manner. In cases where the linear force model fails to predict the machining force accurately, a nonlinear model should be used. A good model for the setup used in this chapter is found to be:

$$F(s) = K \cdot w^{\gamma} \cdot d^{\alpha} \cdot f^{\beta} \tag{8}$$

and

$$F(s) = K \cdot w^{\gamma} \cdot d^{\alpha} \cdot f^{\beta} \frac{1}{\tau_m s + 1} \tag{9}$$

where the constants a, β and γ depend on such factors as tool material, tool geometry, workpiece material, etc. and do not vary significantly during the machining operation. The cause of the nonlinearities is not well understood but is believed to be caused by the strength and temperature of the cutting zone, as well as the resultant force direction, as the process parameters vary. These nonlinear effects have long been recognized and have been mentioned in the force control literature.

3. Chatter Analysis

One of the major hurdles preventing the adoption of robot for machining process is chatter. Tobias (Tobias & Fishwick, 1958) and Tlusty (Tlusty & Polacek, 1963) recognized that the most powerful sources of chatter and self-excitation were the regenerative and mode coupling effects. Regenerative chatter is based on the fact that the tool cuts a surface already cut during the previous revolution, so the cutting force and the depth of cut vary. Mode coupling chatter is due to the fact that the system mass vibrates simultaneously in the directions of the degrees of freedom (DOF) of the system, with different amplitudes and with a difference in phases. Regenerative chatter happens earlier than the mode coupling chatter in most machining processes, as explained by Altintas (Altintas, 2000).
Although extensive research on chatter has been carried out, none of the existing research has focused on chatter mechanism in robotic machining process. The result is that robotic engineers and technicians are frustrated to deal with elusive and detrimental chatter issues without a good understanding or even a rule of thumb guideline. Very often, to get their process working correctly, one has to spend tremendous time on trial and error for the sheer luck of stumbling a golden setup or has to sacrifice the productivity by settling on conservative cutting parameters much lower than the possible machining capability. This section is trying to bridge the gap by pointing out the underline chatter generation mechanism (Pan et al., 2006). First, the characteristics of chatter in robotic machining process are presented, followed by the detailed analysis of chatter mechanism applying both regenerative and mode coupling theory. Further experimental results are then provided to verify the theoretical analysis. Finally stability criteria and insightful guidelines for avoiding chatter in robotic machining process are presented.

3.1 Characteristics of chatter in robotic machining process

Severe low frequency chatter has been observed ever since when robot was first applied in machining process, nevertheless, no theoretical explanation and analysis are available in the existing literature to date. The conventional wisdom is that this is due to the obvious fact that the robot is much less stiffer than CNC machine, but no answer is provided for the further explanation. The reason for this blank may be the lack of enough sensory information, in particular, the process force information. In addition to the surface damage on the workpiece due to chatter marks, the occurrence of severe chatter results in many adverse effects, which may include a poor dimensional accuracy of the workpiece, a reduction of tool life, and a damage to the machine, etc. Certain conservative cutting

parameters, which were proposed by other researchers, intended to avoid chatter at the expense of the loss of productivity.

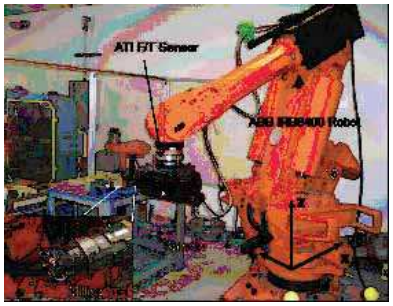

Fig. 3. Setup of robotic end milling.

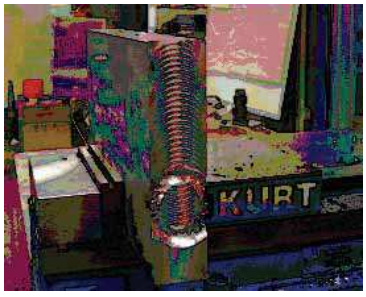

Fig. 4. Chatter marks on the workpiece.

In the present work, a robotic milling work cell is setup with ABB IRB6400 industrial manipulator. The spindle is mounted on robot wrist while the workpiece is fixed on the steel table. An ATI 6DOF Force/Torque sensor is set up between the robot wrist and spindle as shown in Figure 3. After compensating the gravity of spindle and tool, 3 DOF machining force could be measured accurately. When chatter occurs, the amplitude of cutting force increases dramatically and the chatter frequency is observed from the Fast Fourier Transform of force data. The experimental conditions for robotic end milling are summarized in Table 2.

Test	End milling	Deburing
Robot	ABB IRB6400	ABB IRB6400
Workpiece	A2024, L300mm×W38mm×H150mm	A2024, L300mm×W51mm×H150mm
Spindle type	SETCO,5HP, 8000RPM	GCOLOMBO,11HP, 24,000RPM
Tool type	SECO Φ52mm, Round insert, Φ1.89mm×5	SANDVIK, Φ20mm, Helical 2-flute
Cutting fluid	- (Dry cutting)	- (Dry cutting)
Feed rate	30 mm/s	60 mm/s
Spindle speed	3600 RPM	18,000 RPM
DOC	1-4 mm	5mm
WOC	38mm	15mm

Table 2. Experimental conditions for robotic machining

In most situations, the cutting process is stable; the work cell could conduct 4-5mm depth-of-cut (DOC) until reaching the spindle power limit. Nevertheless, while feed in -Z direction, severe low frequency (10Hz) chatter occurs when the DOC is only 2 mm. The characteristics of this low frequency chatter are:

1. The frequency of chatter is the robot base natural frequency at 10Hz. It does not change with the variation of cutting parameters such as spindle speed, width-of-cut (WOC), feed speed and the location of workpiece.
2. When chatter occurs, the entire robot structure start to vibrate. The magnitude of vibration is so large that obvious chatter marks are left on the workpiece surface. (Figure 4)
3. In the cutting setup of Figure 3 and Table 2, using the exact same cutting parameters (DOC, RPM, WOC, Feed speed), chatter starts to occur when feed in –Z

direction, DOC=2mm, while the process is stable when feed in +Z, ±X direction, even with the DOC=4mm. The cutting forces in unstable (feed in –Z direction) and stable (feed in +Z direction) conditions are plotted in Figure 5.

4. The cutting process has different chatter limit at different locations in the robot workspace. Machining experiments are carried out at three different locations along the table, defined as L1, L2 and L3. They have the same Y, Z coordinates and different X coordinate. L1 is the location shown in Figure 3, L3 is on the other corner, and L2 is in the middle. Without changing other cutting parameters, chatter limit for L1 is DOC=2mm, for L2 is DOC=1.5mm, for L3 is DOC=1.1mm.

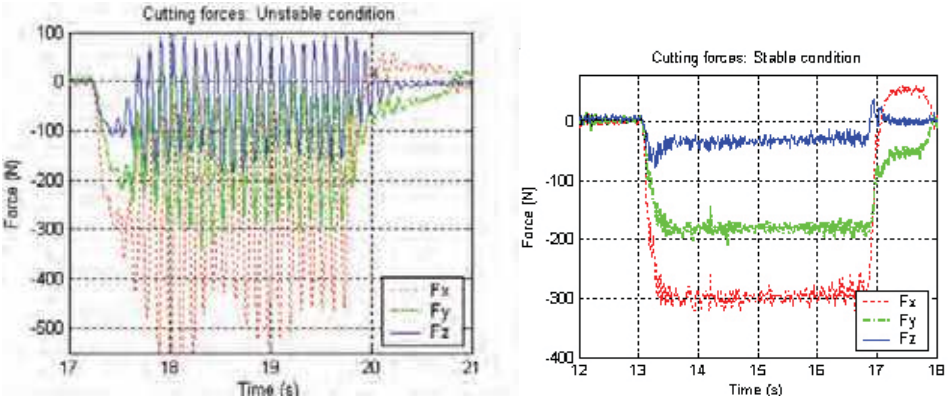

Fig. 5. Cutting force profile. (Left) force plot while low frequency chatter happens, cutting condition listed in Table 2. (Right) force plot while system stable, cutting condition is the same except that feed in opposite direction.

3.2 Chatter analysis based on regenerative mechanism

Regenerative chatter is a self-excited vibration in a machining operation resulting from the interference between the current machining pass and the wavy surface generated during previous machining passes. The energy for the chatter comes from the forward motion of the tool/workpiece. The frequency is typically slightly larger than the natural frequency of the most flexible vibration mode of the machine-tool system. The corresponding mathematical models are delay-differential equations (DDEs) or periodic differential equations (PDFs). Merritt (Merritt, 1965) combined the regenerative theory and a feedback loop to derive a systematic and graphical stability criterion. His approach introduced an elegant new method of stability analysis that was later adopted by many investigators and led to major advances towards the understanding and prediction of the chatter.

A simplified one-DOF analysis could easily prove how regenerative mechanism will not introduce chatter at as low as 10 Hz, while the spindle speed is 3600RPM. The block diagram of one-DOF close loop system is shown in Figure 6. The transfer function of this model is:

$$G(s) = \frac{1}{ms^2 + cs + k + K_p(1 - e^{-s\tau})} \tag{10}$$

where τ is the time delay between the current cut and the previous cut. It is related to the spindle speed and number of teeth on the cutting tool. The stability margin is when the characteristic equation of this transfer function has pure imaginary solutions, which are:

$$d = \frac{m(\omega_c^{\ 2} + 4\omega_n^{\ 2}\zeta^2)}{2K_p} \tag{11}$$

$$\Omega = 60(\frac{\omega_c}{2\phi - \pi(1-2n)}) \qquad n = 1,2,3... \tag{12}$$

where d is DOC, Ω is RPM, $\omega_n = \sqrt{k/m}$, $\zeta = c/2m$, and $\omega_c = \omega_n\sqrt{1-\zeta^2}$. The corresponding stability lobe is plotted in Figure 7. Obviously, with spindle speed $\Omega = 3600$, robot works on the very right side of first stability lobe, where DOC is almost unlimited.

Based on regenerative chatter theory, one would not expect to observe the low frequency chatter. However, from the experimental test, such chatter behavior indeed exists, which forced us to look into other theories to explain the underline mechanism for this kind of chatter. In the following subsection, we would explore the mode coupling chatter theory and find that is the most reasonable explanation to the aforementioned problem.

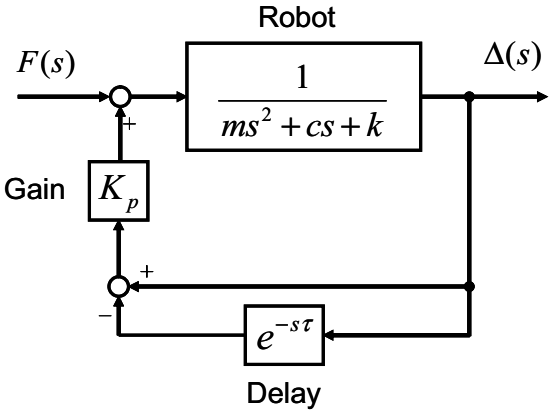

Fig. 6. Block diagram of one-DOF regenerative chatter model.

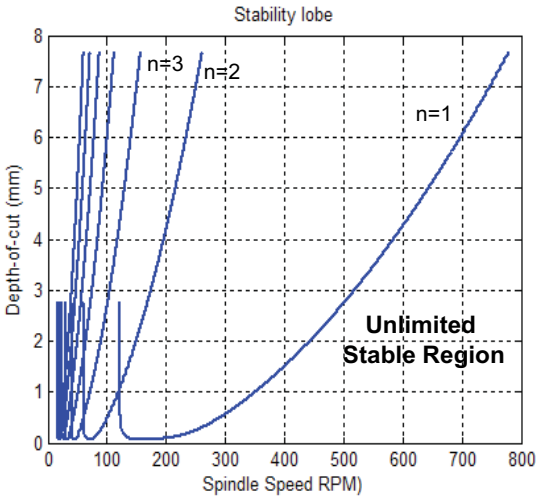

Fig. 7. Stability lobe of robotic end milling.

3.3 Chatter analysis based on mode coupling mechanism

Generally, from Eq. (1) and Eq. (2), the dynamic model of the system is formulated as:

$$[M]\{\ddot{\Delta}\}+[C]\{\dot{\Delta}\}+[K]\{\Delta\}=[K_p]\{\Delta\} \tag{13}$$

The stability of the system depends on the eigenvalues of the equation above. Since the focus here is to analyze the chatter due to the mode coupling effect, the following simplifications are made:

1. Since damping effect will always increase the stability of the system and it is difficult to be identified accurately, we only analyze the undamped system.
2. While round inserts are applied in robotic end milling operation, the machining force in feed direction is much smaller than the forces in cutting and normal direction (Figure 5). Thus while feed in Z direction, we could simplify the analysis into a 2-DOF problem in X-Y frame.

Thus, machining force model become $F = K_p Y$, with F and X form a angle of $\alpha+\gamma$, as shown in Figure 8. The 2-DOF dynamic equation of system without considering the damping effect is:

$$\begin{bmatrix} m_{11} & m_{12} \\ m_{21} & m_{22} \end{bmatrix}\begin{Bmatrix} \ddot{X} \\ \ddot{Y} \end{Bmatrix}+\begin{bmatrix} k_{11} & k_{12} \\ k_{21} & k_{22} \end{bmatrix}\begin{Bmatrix} X \\ Y \end{Bmatrix}=\begin{bmatrix} 0 & K_p\sin(\alpha+\gamma) \\ 0 & K_p\cos(\alpha+\gamma) \end{bmatrix}\begin{Bmatrix} X \\ Y \end{Bmatrix} \tag{14}$$

A similar model was analyzed by Gasparetto (Gasparetto, 1998) for wood cutting application. General solutions for Eq. (13) are available, if the coefficient matrixes are identified accurately. Since mass matrix $[M]$ is symmetric and positive definite, stiffness matrix $[K]$ is symmetric and semi-positive definite, there exists a matrix $[V]$ which achieves

$$[V]^T[M][V]=[I] \tag{15}$$

$$[V]^T[K][V]=[K_\Lambda]=diag(k_1,...,k_n) \tag{16}$$

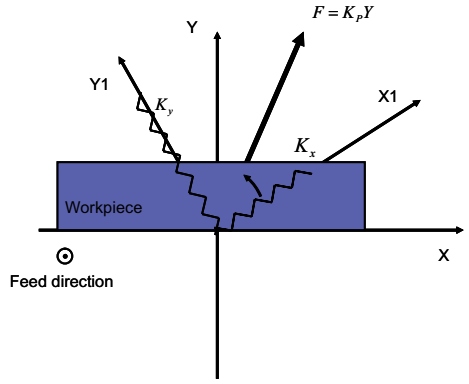

Fig. 8. 2D model of mode coupling chatter system.

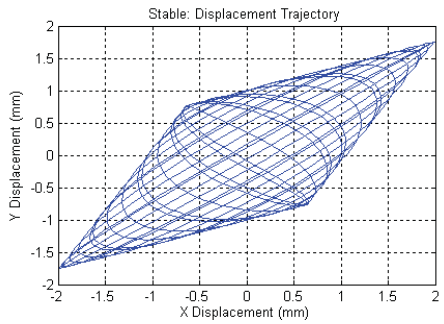

Fig. 9. TCP locus in stable conditionfor undamped system.

By perform this similarity transformation, Eq. (13) becomes

$$\{\ddot{q}\}+[K_\Lambda]\{q\}=[V]^T[K_p][V]\{q\} \tag{17}$$

where

$$\{q\} = [V]^{-1}\{\Delta\} \tag{18}$$

Generally $[V]$ is not an orthogonal matrix; which means the axes of generalized coordinate $\{q\}$ are not perpendicular to each other. The stability of the system depends on the eigenvalues of matrix $[V]^T[K_p][V]-[K_\Lambda]$. If all the eigenvalues of this matrix are negative real number, the system is stable; otherwise, if this matrix has complex eigenvalues, the system will be unstable.

For better explanation of the problem, without loss of generality, we assume that $[M]$ is diagonal without transformation and model mass for each direction is the same

$$[M] = \begin{bmatrix} m & 0 \\ 0 & m \end{bmatrix} \tag{19}$$

In this case, $[V]$ is an orthogonal matrix, that is $[V]^T = [V]^{-1}$, similarity transformation is equal to rotation of the original frame. Thus, the uncoupled principle stiffness directions are perpendicular to each other. In figure 8, X and Y represent frame $\{\Delta\}$; X_1 and Y_1 represent frame $\{q\}$. Cutting process is operated in frame $\{\Delta\}$ with cutting force in X direction and normal force in Y direction (direction of DOC). In frame $\{q\}$, both $[M]$ and $[K]$ are diagonal. The transformation from $\{\Delta\}$ to $\{q\}$ is defined as $\{q\} = [V]^{-1}\{\Delta\}$, where

$$[V]^{-1} = \begin{bmatrix} \cos(\alpha) & \sin(\alpha) \\ -\sin(\alpha) & \cos(\alpha) \end{bmatrix} \tag{20}$$

Then the system equation in the frame $\{q\}$ is:

$$\begin{bmatrix} M & 0 \\ 0 & M \end{bmatrix}\begin{Bmatrix} \ddot{X}_1 \\ \ddot{Y}_1 \end{Bmatrix} + \begin{bmatrix} K_x & 0 \\ 0 & K_y \end{bmatrix}\begin{Bmatrix} X_1 \\ Y_1 \end{Bmatrix} = \begin{bmatrix} K_p\cos(\gamma)\sin(\alpha) & K_p\cos(\gamma)\cos(\alpha) \\ K_p\sin(\gamma)\sin(\alpha) & K_p\sin(\gamma)\cos(\alpha) \end{bmatrix} \cdot \begin{Bmatrix} X_1 \\ Y_1 \end{Bmatrix} \tag{21}$$

Eq. (21) could be rearranged to give:

$$\begin{Bmatrix} \ddot{X}_1 \\ \ddot{Y}_1 \end{Bmatrix} = \begin{bmatrix} \dfrac{K_p\cos(\gamma)\sin(\alpha) - K_x}{M} & \dfrac{K_p\cos(\gamma)\cos(\alpha)}{M} \\ \dfrac{K_p\sin(\gamma)\sin(\alpha)}{M} & \dfrac{K_p\sin(\gamma)\cos(\alpha) - K_y}{M} \end{bmatrix} \cdot \begin{Bmatrix} X_1 \\ Y_1 \end{Bmatrix} \tag{22}$$

Let

$$K_x^{'} = K_x - K_p\cos(\gamma)\sin(\alpha)$$
$$K_y^{'} = K_y - K_p\sin(\gamma)\cos(\alpha)$$

The characteristic equation of Eq. (22) is:

$$\lambda^4 + \frac{K_x^{'} + K_y^{'}}{M}\cdot\lambda^2 + \frac{K_x^{'}K_y^{'} - \frac{1}{4}K_p^2\sin(2\gamma)\sin(2\alpha)}{M^2} = 0 \tag{23}$$

The solution of Eq. (23) gives:

$$\lambda^2 = \frac{-(K_x^{'} + K_y^{'}) \pm \sqrt{(K_x^{'} - K_y^{'})^2 + K_p^2\sin(2\gamma)\sin(2\alpha)}}{2M} \tag{24}$$

In practice, $K_x, K_y >> K_p$ is always satisfied, otherwise, cutting process could not be executed. Thus $K_x^{'} \approx K_x$ and $K_y^{'} \approx K_y$.

If $(K_x^{'} - K_y^{'})^2 + K_p^2 \sin(2\gamma)\sin(2\alpha) > 0$, then the two λ^2 are real negative numbers. In this case the four eigenvalues of the system located on the imaginary axis, symmetric with respect to real axis. The solution of system is Lissajous curves as shown in Figure 9. The system results stable in a BIBO sense. Moreover, since the system damping always exist, the structure damping of the real system will shift the eigenvalues of the system toward left in the complex plan, therefore giving exponentially decaying modes.

If $(K_x^{'} - K_y^{'})^2 + K_p^2 \sin(2\gamma)\sin(2\alpha) < 0$, then two λ^2 are complex number with negative real part. In this case the four eigenvalues of the system are located symmetrically with respect to the origin of the complex plane, so two of them have positive real part. Therefore, instability occurs in this case. The solution of system is exponential increasing as shown in Figure 10. While the damping effect is considered, the locus of TCP is an ellipse.

Unstable region could be represented as:

$$\sin(2\gamma) < \frac{[K_x - K_y + K_p \sin(\gamma - \alpha)]^2}{-K_p^2 \sin(2\alpha)} \tag{25}$$

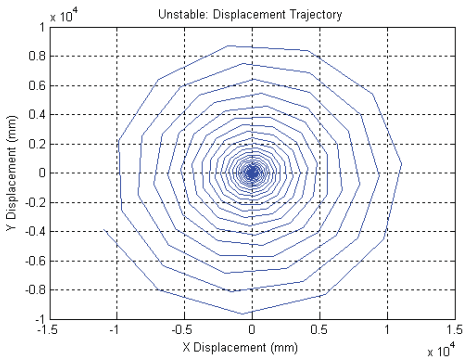

Fig. 10. TCP locus in unstable condition for undamped system.

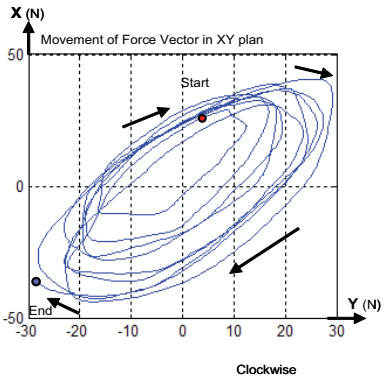

Fig. 11. Locus of force vector while chatter happens.

An important result here is that unstable condition is only possible when $K_p > |K_x^{'} - K_y^{'}|$. That means the mode coupling chatter only occurs when the process stiffness is larger than the difference of two principle stiffness of robot. The physical meaning of the equation gives us the general stability criterion. If a machining system can be modeled by a two degree of freedom mass-spring system, the dynamic motion of the TCP can take an elliptical path. If the axis with the smaller stiffness lies within the angle formed by the total cutting force and the normal to the workpiece surface, energy can be transferred into the machine-tool structure, thus producing mode coupling chatter. The depth of cut for the threshold of stable operation is directly dependent upon the difference between the two principal stiffness values, and chatter tends to occur when the two principal stiffness are close in magnitude.

For CNC machine, the structure stiffness k is on the level of 10^8 N/m, and the process stiffness K_p is usually in the range of $10^5 \sim 10^6$ N/m. As a result, any small difference of k

in each principle directions is much larger than K_p. Before the occurrence of mode coupling chatter, spindle power limit or regenerative chatter limit already reached.

The story is totally different for industrial robot, where stiffness k is on the level of 10^6 N/m and has close magnitude in each direction. Since the process stiffness K_p of machining aluminum workpiece is usually on the level of 10^5 N/m, the mode stiffness of each principle direction could be smaller than process stiffness in certain robot configuration. The mode coupling chatter will then occur even in very light cutting condition. The vibration limit of robotic milling operation depends on the relative angels between machining force vector and the direction of the principle mode stiffness.

The above analysis also coincide with a rule of thumb in the machine tool industry, that the stiffness of two directions should at least has 10% difference to prevent chatter. The characteristics of low frequency chatter summarized in section 3.1 be perfectly explained by mode coupling mechanism:

1. The frequency of mode coupling chatter is the same as the base frequency of the machine. The process parameters such as spindle speed, width-of-cut (WOC), and feed speed won't change the frequency of chatter.
2. In unstable condition, the solution of the system will exponentially increase until it is balanced by damping effects or just crash (Figure 4). The locus of force vector is drawn in Figure 11. The locus of tool tip movement will take the same elliptical path.
3. An unstable cutting process could become stable by only changing the feed direction because the direction of force vector is changed while machine structure keeps the same.
4. Chatter limit of the process is configuration dependent due to the coupled robot structure. The mass matrix and stiffness matrix are not constant; they take different values at different robot configurations. As a result, although the force vector is the same, the chatter limit is different since the machine structure is different.

3.4 Experimental results and analysis

Further experimental verification of the theoretical analysis described in the foregoing subsection was observed in robotic deburing tests. The same type of robot is applied for deburing test of aluminum workpiece as shown in Figure 12; the detailed cutting condition is given in Table 3.

Fig. 12. Setup for robotic deburing.

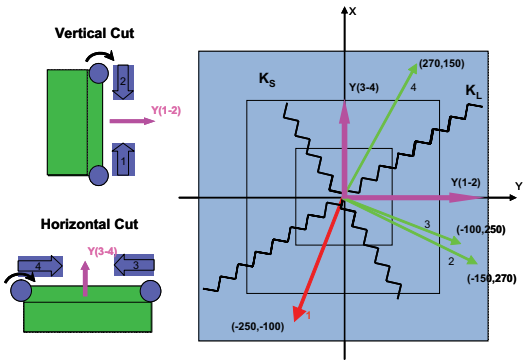

Fig. 13. Stability analysis of deburring.

	Feed direction	Milling type	Force X direction (N)	Force Y direction (N)	Stability
Case 1	+X	Up-milling	-250	-100	Chatter
Case 2	-X	Down-milling	-150	270	Stable
Case 3	-Y	Up-milling	-100	250	Stable
Case 4	+Y	Down-milling	270	150	Stable

Table 3. Summary of deburing test.

In the deburing test, side milling using two-flute helical mill were carried out. Figure 13 presents four machining cases with exactly same cutting parameters except for different feed direction. The cutting conditions and measured machining forces are listed in table 3. Experimental results show that chatter only happens in case 1, while the processes are stable for the rest of the cases. In Figure 13, four force vectors are plotted in the fixed frame X-Y, K_S and K_L represent the smaller and larger principle stiffness of robot calculated from robot structure model, $Y(1-2)$ and $Y(3-4)$ represent the normal direction to the workpiece in vertical and horizontal cutting tests. From the stability criteria established in section four, mode coupling chatter will occur when axis with the smaller stiffness lies within the angle formed by the total cutting force and the normal to the workpiece surface. From Figure 13, stability criteria predict that chatter will only occur in case 1, which perfectly matches the experimental results.

Another important result worth mentioning here is the effect of up-milling and down-milling on mode coupling chatter in robotic machining process. As shown in Figure 14, the direction of cutting force is in a range that is perpendicular to the normal of workpiece in up-milling while the direction of cutting force is almost the same as normal of workpiece in down-milling. Thus, it is more likely for axis with the smaller stiffness to lie between the force vector and the workpiece normal direction during up-milling than down-milling. As a result, from chatter point of view, down-milling is preferred for robotic machining process.

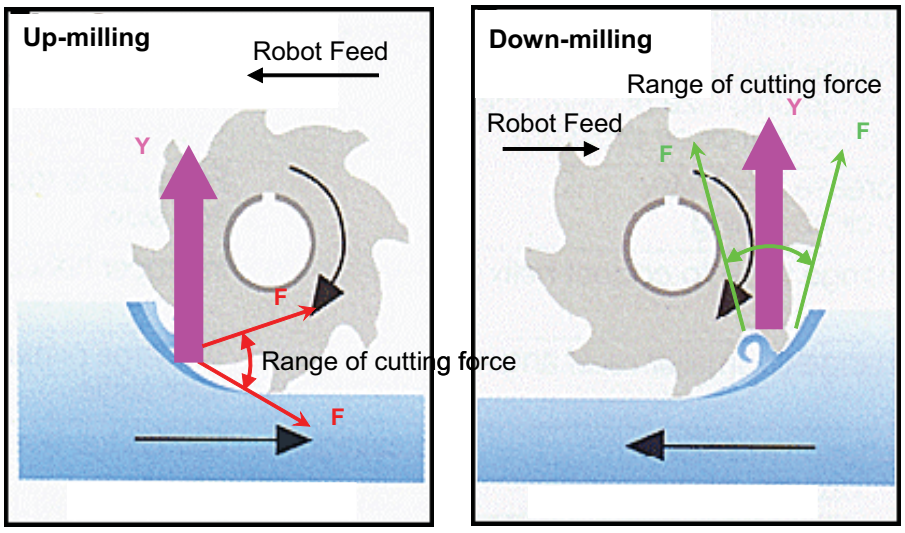

Fig. 14. Up-milling vs. down-milling in mode coupling chatter analysis.

After investing the intrinsic mechanism of low frequency chatter, practical guidelines for chatter-free robotic machining process is summarized here.

1. Select the proper cutting tool. The tool or inserts with different geometry will distribute machining force to different directions. Round insert always generates larger normal force (DOC direction) compared to square insert with zero degree lead angle. Since DOC is the most sensitive parameter related to machining force, chatter may arise more easily if the process has larger normal force. Thus Round insert is not recommended for robotic machining although it has many advantages and is widely using by CNC machine.
2. Plan the proper work space. Since the robot displays different mechanical properties, which are mass, stiffness and damping, at different locations in the workspace, selecting a proper machining location that will have higher chatter limit.
3. Plan the proper path and feed direction. Changing the feed direction is the easiest way to re-direct machining force without affecting the existing setup. Based on the theoretical analysis and experimental results, this is an effective method to avoid mode coupling chatter in many situations.
4. Chatter is more likely to occur in up-milling rather than in down-milling in robotic machining process.

4. Deformation Compensation

Field tests using industrial robots for heavy machining such as milling often found that a perfect robot program without considering contact and deformation fails to produce the desired path once the robot starts to execute the machining task. While thermal induced error is the largest error component for CNC machining, motion error contributes most of the total machining errors in robots. For example, a 500N cutting force during a milling process will cause a 1 mm position error for a robot instead of a less than 0.01mm error for a CNC machine. The major motion error sources in robotic machining process can be classified into two categories, (1) Machining force induced error, and (2) robot inherent motion error (kinematic and dynamic errors, etc.). The inherent motion error, typically in the range of 0.1 mm, is resulted from the robot position controller and would appear even in non-contact cases. While the machining force in the milling process is typically over several hundreds of Newton, the force-induced error, which could easily go up to 1 mm, is the dominant factor of surface error. In order to achieve higher dimensional accuracy in robotic machining, the deformation due to the interactive force must be accurately estimated and compensated in real time.

The existing research of robot deformation compensation is focused on gravity compensation, deflection compensation of large flexible manipulators, etc. Not much attention has been paid to the compensation of process force induced robot deformation due to the lack of understanding and model of robot structure stiffness, the lack of real time force information and limited access to the controller of industrial robot.

4.1 Identification of robot stiffness model

Since force measurement and subsequent compensation is carried out in 3-D Cartesian space, a stiffness model, which relates the force applied at the robot tool tip to the

deformation of the tool tip in Cartesian space, is crucial to realize deformation compensation. The model should be accurate enough for the prediction of robot structure deformation under arbitrary load conditions. At the same time, it needs to be simple enough for real time implementation. Detailed modelling of all the mechanical components and connections will render a model too complicated for real-time control, and difficult for accurate parameter identification. The stiffness model in section 2 is an ideal candidate for the deformation compensation. Based on this model, the estimated tool tip deformation in Cartesian space subject to force *F* can be written as:

$$\Delta X = J(Q)K_q^{-1}J(Q)^T \cdot F \tag{26}$$

Experimental determination of joint stiffness parameters is critical in fulfilling real-time position compensation. Since the joint stiffness is an overall effect contributed by motor, joint link, and gear reduction units, it is not realistic to identify the stiffness parameter of each joint directly by dissembling the robot. The practical method is to measure it in Cartesian space.

To be able to measure small deformations in 3-D space, the end-effector is equipped with a sphere-tip tool shown in figure 15. The tool tip is set to a fixed point in the workspace, and the manipulator joint values are recorded. A given load in the range of 100N~400N is applied to the tool, causing the sphere-tip to move away from the original point. The original and deformed positions are measured with ROMER, a portable CMM 3-D digitizer, and the 3-DOF translational deformations are calculated. From Eq. (26), K_q could be solved by least square method. The same experiment was repeated at several different locations in the robot workspace. As can be seen from figure 16, the deviation of the results at different test locations is small, which means a set of constant parameters could model the robot deformation with small error.

Fig. 15. Experiment Setup for robot stiffness measurement.

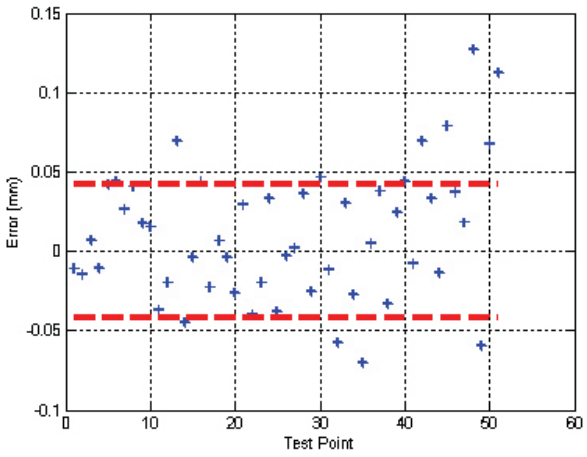

Fig. 16. Error of stiffness modeling.

4.2 Real-time deformation compensation

Figure 17 shows the block diagram of real time deformation compensation. After filtering the force sensor noise and compensating the gravity of the spindle and the tool, the force signal was translated into the robot tool frame. Based on the stiffness model identified before, the deformation due to machining force is calculated in real time and the joint reference for the robot controller is updated.

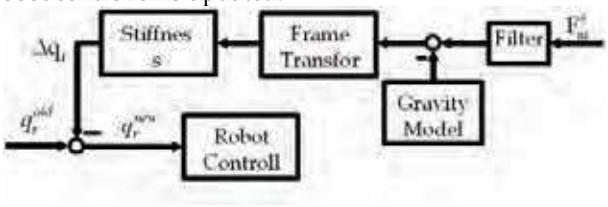

Fig. 17. Principle of real-time deformation compensation.

Fig. 18. Experimental setup for robotic milling.

4.3 Experimental results

A robotic milling cell, where an ABB IRB6400 robot holds a spindle as shown in figure 18, is used for deformation compensation test. For illustration purpose, the workpiece is chosen as a 6063 aluminum block. A laser displacement sensor is used to measure the finished surface. The surface error without deformation compensation demonstrates counter-intuitive results; an extra 0.5mm was removed in the middle of the milling path. Conventional wisdom says that a flexible machine would also cut less material due to deformation, since the normal force during cutting will always push the cutter away from the surface and cause negative surface error. However, in the articulated robot structure, the deformation is also determined by the structure Jacobian, in a lot of cases, a less stiff robot could end up cutting more material than programmed. The coupling of the robot stiffness model explains this phenomenon, the force in feed direction and cutting direction will result in positive surface error in that robot configuration. Since the feed force and the cutting force are the major components in this setup, the overall effect will cut the surface 0.5 mm more than the commanded depth. In our definition, negative surface error means less material was removed than the commanded position.

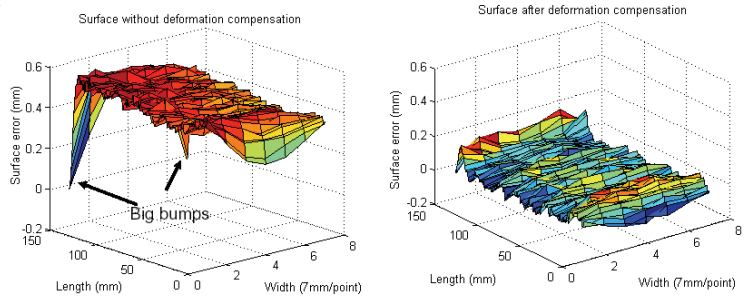

Fig. 19. Deformation compensation results

The result after deformation compensation shows a less than 0.1 mm surface error, which is in the range of robot path accuracy (Figure 19). Further test conducted on the foundry cylinder head workpiece shows that the surface accuracy improved from 0.9mm to 0.3mm, which is below the 0.5mm target accuracy for pre-machining application.

5. Controlled Material Removal Rate

In pre-machining processes, maximum material removal rates are even more important than precision and surface finish for process efficiency. MRR is a measurement of how fast material is removed from a workpiece; it can be calculated by multiplying the cross-sectional area (width of cut times depth of cut) by the linear feed speed of the tool:

$$MRR = w \cdot d \cdot f \tag{27}$$

Where w is width of cut (mm), d is depth of cut (mm), f is feed speed (mm/s).

Conventionally, feed speed is kept constant in spite of the variation of depth of cut and width of cut during foundry part pre-machining process. Since most foundry parts have irregular shapes and uneven depth of cut, this will introduce a dramatic change of MRR, which would result in a very conservative selection of machining parameters to avoid tool breakage and spindle stall. The concept of MRR control is to dynamically adjust the feed

speed to keep MRR constant during the whole machining process. As a result, a much faster feed speed, instead of a conservative feed speed based on maximal depth of cut and width of cut position, could be adopted (Figure 20).

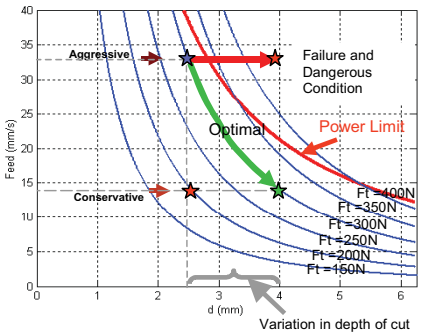

Fig. 20. Controlled material removal rate.

Since the value of MRR is difficult to measure, the MRR is controlled by regulating the cutting force, which is readily available in real-time from a 6-DOF strain gage force sensor fixed on the robot wrist. Placing the analysis of the material removal process on a quantitative basis, the characterization of cutting force is important for research and development into the modeling, optimization monitoring and control of metal cutting.

The challenges for designing a robust controller for MRR is the fact that cutting process model varies to a large degree depending on the cutting conditions. Efforts for designing an adaptive controller will be presented in a separate paper.

As the feed speed f is adjusted to regulate the machining force, MRR could be controlled under a specific spindle power limit avoiding tool damage and spindle stall. Also, controlled MRR means predictable tool life, which is very important in manufacturing automation. Figure 21 shows the block scheme of machining force control with controlled material removal rate (CMRR). For the force process model represented in Eq.(7), with the proper selection of reference feed speed f_r and reference force F_r, a PI controller is adopted to regulate the cutting force F_c, while force process gain θ changes.

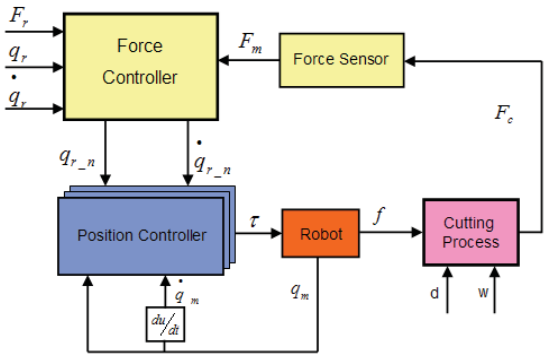

Fig. 21. Force control for robotic machining.

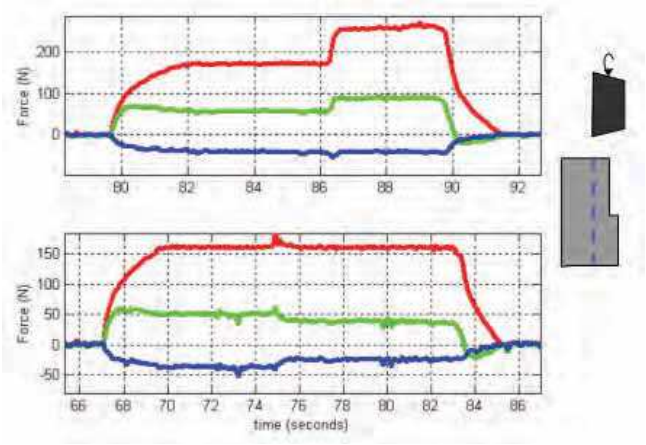

Fig. 22. Force control result of variant depth of cut.

The same workcell shown in figure 18 is used for MRR test. A 6063 aluminum block is intentionally machined to look like in Figure 22 to simulate the variation of cut depth. Tests on an aluminum block with the depth of cut changed from 2 mm to 3 mm shows, when force control is activated, the cutting force is regulated in spite of the variance of depth of cut (Figure 22). The milling test of aluminum with variation of width of cut shows similar results.

As a result, the feed speed could always be setup as fast as the limit of spindle power. In a foundry parts milling or deburring process, the robot won't have to move at a very conservative speed to avoid tool breakage or spindle stall. The cycle time decreased by CMMR is typically around 30% to 50% for different workpieces.

6. Summary and Conclusion

This chapter presents critical issues and methodologies to improve robotic machining performance with flexile industrial robots. The problems under the investigation are low frequency chatter, machining force induced robot deformation and conservative feed rate for non-uniform cutting depth and width, which are often the causes of unacceptable quality, lower productivity, and process instability. For low frequency chatter, it was found that mode-coupling chatter is the dominant source, largely due to the inherent low structure stiffness of industrial robot. The occurrence of mode coupling chatter depends on the relative orientation of the machining force vector and the principle stiffness axes of the robot. Methods such as changing the feed direction, using different robot configuration or changing another type of tool are recommended to avoid chatter occurrence. To address deformation problem, stiffness modeling and real time deformation compensation were adopted for robot control. A constant joint stiffness model, which accounts for the dominant contribution of joint compliance to the tool center point (TCP) deflection, was chosen to minimize the computation time. Test results showed 0.5mm surface error improvement after the compensation. To improve the efficiency in machining parts with uneven cut depth and width, a PI control strategy was proposed to adjust the cutting feed rate based on the measured cutting force. The feed rate was optimized in real time to compensate process

variations to help maximize material removal rate (MRR) and minimize cycle time. Practical machining experiments conducted in the lab showed great reduction of cycle time, as well as better surface accuracy. These results outline a promising and practical use of industrial robots for machining applications that is not possible at present.

7. References

Akbari, A. & Higuchi, S. (2000). Autonomous tool adjustment in robotic grinding, *The International conference on Precision Engineering*(ICoPE) ,pp.121-126

Altintas, Y. (2000). *Manufacturing Automation: Metal Cutting Mechanics, Machine Tool Vibrations, and CNC Design*, 1st ed., Cambridge University Press, NY, USA

Budak, E. & Altintas, Y. (1998). Analytical prediction of chatter stability conditions for multi-degree of systems in milling. Part I: modeling, Part II: applications. *Transactions of ASME, Journal of Dynamic Systems, Measurement and Control*, Vol.120, pp.22-36

Chen, Y. & Hu, Y. (1999). Implementation of a robot system for sculptured surface cutting. Part 1. rough machining. *International Journal of Advanced Manufacturing Technology*, Vol. 15, pp. 624-629

Daneshmend, L. & Pak, H. (1986). Model reference adaptive control of feed force in turning, *ASME Journal of Dynamic Systems, Measurement, and Control*, Vol. 108, No. 3, pp. 215-222.

Gasparetto, A. (1998), A system theory approach to mode coupling chatter in machining, *ASME Journal of Dynamic Systems, Measurement, and Control,* Vol. 120, pp.545-547.

Kim, S.; Landers, R. & Ulsoy, G. (2003). Robust machining force control with process compensation. *Journal of Manufacturing science and engineering*, Vol. 125, pp. 423-430

Matsuoka, S., Shimizu, K., Yamazaki, N. & Oki, Y. (1999). High-speed end milling of an articulated robot and its characteristics, *Journal of Materials Processing Technology*, Vol. 95, No. 1-3, pp. 83-89

Merritt, H. (1965). Theory of self-excited machine tool chatter: contribution to machine-tool chatter research-1, *ASME Journal of Engineering for Industry*, Vol. 87, No. 4, pp. 447-454

Pan, Z. ; Zhang, H. ; Zhu, Z. ; Wang, J. (2006). Chatter analysis of robotic machining process, *Journal of Materials Processing Technology*, Vol.173, pp.301-309

Sallinen, M. & Heikkilä, T. (2000). Flexible workobject localisation for CAD-based robotics, *Proceedings of SPIE Intelligent Robots and Computer Vision XIX: Algorithms, Techniques, and Active Vision*, Vol.4197, pp. 130 – 139, Boston, USA, Nov. 2000

Stein, J. & Huh, K. (2002). Monitoring cutting forces in turning: a model-based approach. *Journal of Manufacturing science and engineering*, Vol. 124, pp. 26-31

Tlusty, J. & Polacek, M. (1963). The stability of machine tools against self excited vibrations in machining, *International Research in Production Engineering*, *ASME*, pp. 465-474.

Tobias, S., & Fishwick, W. (1958). The chatter of lath tools under orthogonal cutting conditions, *The Transaction of the ASME*, No. 80, pp. 1079–1088

Wang, J. ; Sun, Y. & et. al. (2003a). Process modeling of flexible robotic grinding, *International Conference on Control, Automation and Systems,* Gyeongju, Korea, Oct. 2003

Wang, J. ; Sun, Y. & et. al. (2003b). In-process relative robot workcell calibration, *International Conference on Control, Automation and Systems,* Gyeongju, Korea, Oct. 2003

Whitney, D. (1977). Force feedback control of manipulator fine motions, *ASME Journal of Dynamic Systems, Measurement, and Control*, Vol. 99, No. 2, pp. 91–97

Yang, S. (1996). Real-time compensation for geometric, thermal, and cutting force induced errors in machine tools. *Ph.D. dissertation*, The University of Michigan

Zhang, H. & et. al., (2005). Machining with flexible manipulator: toward improving robotic machining performance, *IEEE/ASME International Conference on Advanced Intelligent Mechatronics (AIM)*, California, USA, July 2005.

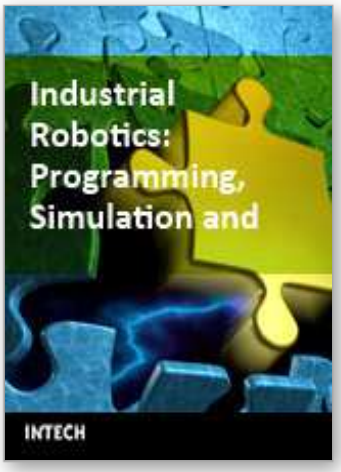

Industrial Robotics: Programming, Simulation and Applications

Edited by Low Kin Huat

ISBN 3-86611-286-6

Hard cover, 702 pages

Publisher Pro Literatur Verlag, Germany / ARS, Austria

Published online 01, December, 2006

Published in print edition December, 2006

This book covers a wide range of topics relating to advanced industrial robotics, sensors and automation technologies. Although being highly technical and complex in nature, the papers presented in this book represent some of the latest cutting edge technologies and advancements in industrial robotics technology. This book covers topics such as networking, properties of manipulators, forward and inverse robot arm kinematics, motion path-planning, machine vision and many other practical topics too numerous to list here. The authors and editor of this book wish to inspire people, especially young ones, to get involved with robotic and mechatronic engineering technology and to develop new and exciting practical applications, perhaps using the ideas and concepts presented herein.

InTech Europe

University Campus STeP Ri
Slavka Krautzeka 83/A
51000 Rijeka, Croatia
Phone: +385 (51) 770 447
Fax: +385 (51) 686 166
www.intechopen.com

InTech China

Unit 405, Office Block, Hotel Equatorial Shanghai
No.65, Yan An Road (West), Shanghai, 200040, China
中国上海市延安西路65号上海国际贵都大饭店办公楼405单元
Phone: +86-21-62489820
Fax: +86-21-62489821